A Quasiclassical Trajectory Study of the Reaction H + O_2 ⇔ OH + O with the O_2 Reagent Vibrationally Excited

Ronald J. Duchovic* and Marla A. Parker†

Department of Chemistry, Indiana University Purdue University at Fort Wayne, Fort Wayne, Indiana 46805-1499

Received: February 1, 2005; In Final Form: April 6, 2005

Quasiclassical trajectories have been computed on the Melius−Blint (MB) Potential Energy Surface (PES) and on the Double Many-Body Expansion (DMBE) IV PES of Pastrana et al. describing the H + O_2 ⇔ OH + O reaction with the nonrotating ($J = 0$) O_2 reagent vibrationally excited to levels $v = 6$, 7, 8, 9, and 10 at four temperatures: 1000, 2000, 3000, and 4000 K. The vibrational energy levels were selected by using a semiclassical Einstein−Brillouin−Keller (EBK) quantization procedure while the relative translational energy was sampled from a Boltzmann weighted distribution. The rate coefficient for the formation of the OH + O products is seen to increase monotonically with quantum number and nearly monotonically with temperature. On the MB PES, at $T = 1000$ K, the total rate coefficient increases by a factor of 5.2 as the initial vibrational quantum number of the O_2 diatom increases from $v = 6$ to $v = 10$. For $T = 2000$ K, this factor drops to 3.3, to 2.9 for $T = 3000$ K, and to 2.5 for $T = 4000$ K. On the DMBE IV PES, at $T = 1000$ K the total rate coefficient increases by a factor of 4.1 as the initial vibrational quantum number of the O_2 diatom increases from $v = 6$ to $v = 10$. For $T = 2000$ K, this factor drops to 3.5, to 2.1 for $T = 3000$ K, and to 2.0 for $T = 4000$ K. The less-direct group (defined below) of trajectories is sensitive to the initial O_2 vibrational excitation in several different temperature ranges, apparently retaining the effect of reagent vibrational excitation. The more-direct group (defined below) of trajectories does not exhibit this behavior. Reagent vibrational excitation does not increase the total rate coefficients for the title reaction more than the increase due to a simple temperature increase. The less-direct and more-direct groups of trajectories differ in their contribution to the rate coefficient for the title reaction. In particular, at $T = 4000$ K, the two PESs used in this work differ dramatically in the roles of the less-direct and more-direct trajectories. The behavior of the more-direct and less-direct groups of trajectories can be understood in terms of the efficiency of intramolecular vibrational energy transfer. This work utilizes the recently introduced PES Library, POTLIB 2001, which made the comparisons between the two PESs discussed in this work possible in a very straightforward way.

I. Introduction

Excited molecules often exhibit very different reactive characteristics than do ground-state molecules because the available internal energy can be utilized to overcome barriers to reaction. While electronically excited molecules have been studied extensively, it has been more difficult to produce vibrationally excited molecules experimentally.[1] However, the effect of reagent vibrational excitation on the rates of chemical reactions has been a subject of extensive interest to the chemical dynamics community for more than thirty years.[1−12] Considerable effort has focused on simple bimolecular reactions of the form A + BC as well as reactions which involve polyatomic reagents.[13] In a previous study[14] it was shown that at specific energies the assumption of vibrational adiabaticity is very good for exothermic reactions involving "early" barriers and for thermoneutral reactions in which the barrier is located midway along the MEP (minimum energy path) connecting reactants and products.

Previous work focused on direct abstraction reactions. Only very recently[12] has there been a comparable study of addition−elimination reactions that are characterized by deep energetic wells on the potential energy surface (PES) which support long-lived addition complexes. Such a reaction is

$$H + O_2 \leftrightarrow HO_2^{\bullet} \leftrightarrow OH + O \qquad (1)$$

that proceeds with no barriers in the forward direction via a relatively deep potential energy well. Reaction 1 plays a crucial role in fundamental combustion processes, with the forward direction being prototypical of a radical−diatom reaction occurring without a potential energy barrier on a single PES. This forward direction of reaction 1 has been characterized as the most important step in combustion[15] and is the primary step initiating the chain branching phenomenon in the oxidation of molecular hydrogen and the oxidation of hydrocarbon fuels. In addition to combustion processes, the reverse direction of reaction 1 plays a critical role in both atmospheric chemistry and interstellar chemistry. In the upper stratosphere and mesosphere, ozone chemistry is controlled by catalytic reactions involving "odd-hydrogen" HO_x (where $x = 0$, hydrogen; $x = 1$, hydroxyl; $x = 2$, hydroperoxyl).[16,17] As a result, the reverse direction of reaction 1 plays a key role in models of atmospheric chemistry describing ozone concentrations.

In recognition of its critical importance, reaction 1 has been the subject of numerous experimental studies focusing on

*Address correspondence to this author. E-mail:duchovic@ipfw.edu.
† Student research assistant, Department of Chemistry, Indiana University Purdue University Fort Wayne, Fort Wayne Indiana 46805-1499.

10.1021/jp050561i CCC: $30.25
Published on Web 06/15/2005

spectroscopic measurements,[10−33,35−53] thermodynamic measurements,[54−56] and dynamical measurements.[57−71] Several compendia[72−74] of recommended rate coefficients for reaction 1 have been compiled based on this extensive experimental work. Complementing the intense experimental activity, there has been a number of ab initio[75−87] and theoretical dynamical[88−131,133−136] studies of this reaction. In total, these investigations now span more than a quarter century.

In the early to mid-1990s, three quantum mechanical studies of reaction 1 were completed using the DMBE IV PES of Pastrana et al.[82] Leforestier and Miller[120] and Viel, Leforestier, and Miller[121] calculated the cumulative reaction probability for reaction 1 using a rigorous three-dimensional quantum mechanical method for $J = 0$. Higher values of J were estimated by using a *J*-shifting approximation and a J_z-conserving approximation. The first work showed agreement with experimental rate coefficients in the range 800 K $\leq T \leq$ 3000 K while the second reported very good overall agreement with the coupled channel calculations of Pack et al.[116] Germann and Miller[122] used flux−flux autocorrelation function methods to compute rate coefficients for reaction 1 in the range 500 K $\leq T \leq$ 2000 K. Again, good agreement with experiment was achieved; nonzero values of the total angular momentum were approximated by using the *J*-shifting technique. In subsequent work, Skinner, Germann, and Miller[123] used a helicity-conserving approximation to calculate quantum mechanical rate coefficients for reaction 1 with total angular momentum $J > 0$. They demonstrated that the much simpler *J*-shifting approximation is a reasonably accurate description of reaction 1, provided an appropriate choice of reference geometry is made.

In a series of investigations Dobbyn et al.[124,125,127] and Song et al.[126] have studied the bound states of HO_2 and the unimolecular decay of HO_2 to H + O_2, comparing three-dimensional quantum calculations (a time-independent scattering approach) with various statistical theories. Dobbyn et al. observe that the HO_2 states are highly mixed and that the underlying classical mechanics is chaotic, implying that the HO_2 is irregular, especially at energies near the dissociation threshold to H + O_2. Their work suggests that there will be a free exchange of energy among the vibrational modes of the HO_2 system, with possible "vague tori" or bottlenecks not significantly affecting the rate of IVR. The calculated quantum RRKM dissociation rates are in excellent agreement with the classical RRKM rate. That is, the quantum mechanical calculations confirm the frequently expressed speculation that RRKM dissociation rates are, on average, equal to the quantum mechanical rates in the "strong coupling" or ergodic limit. Song et al. used four different models (three semiclassical and one quantum mechanical) to calculate HO_2 dissociation rates. The separable EBK model yielded an RRKM rate coefficient in very good agreement with the quantum mechanical calculation that retained full coupling among the vibrational modes, demonstrating that anharmonic coupling between the modes orthogonal to the reaction path is not important in HO_2 dissociation.

Meijer and Goldfield[128−130,133] and Bajeh et al.[131] have studied reaction 1 theoretically using a time-dependent wave packet method on parallel computers and experimentally using a pulsed laser pump−probe technique. Meijer and Goldfield observed that, at higher energies, the total reaction probability decreases as the value of *J* (the total angular momentum quantum number) increases. Their quantum mechanical calculation of reactive cross sections as a function of the relative translational energy of the reactants exhibits excellent agreement with the quasiclassical trajectory−vibrational energy quantum mechanical threshold (QCT-VEQMT) results of Varandas.[17] It should be noted that this level of agreement depends on the imposition of stringent zero-point energy constraints in the QCT-VEQMT method. When a less-restrictive treatment of zero-point energy is applied (QCT-IEQMT method of Varandas[17]), the agreement between the quasiclassical trajectory results and the quantum calculations of Meijer and Goldfield[130] is poor. The issue of zero-point energy will be discussed at greater length below.

Meijer and Goldfield[129] also reported that their calculated quantum mechanical cross sections, at almost every energy, were lower than corresponding experimental results. Bajeh et al. reported experimental cross sections based on monitoring O-atom production in the products of reaction 1, which indicates a much less pronounced variation as a function of reactant relative translational energy. In particular, the relatively sharp increase in reactivity between 115.8 (1.2 eV mol^{-1}) and 164.0 kJ mol^{-1} (1.7 eV mol^{-1}) observed in previous experimental studies[50,52,53] was very clearly absent from the experimental data; this same sharp increase was also absent from the quantum mechanical calculations ($v = 0$) of Meijer and Goldfield.

In a number of the studies briefly summarized above, the *J*-shifting approximation was employed to reduce the complexity of the quantum mechanical calculations. This approximation treats the effect of the centrifugal barrier induced when $J > 0$ by simply introducing an energy threshold that causes the reaction probability to be shifted to higher energies with respect to the corresponding $J = 0$ case. Compared to other approximate quantum mechanical methods (e.g. the helicity conserving approximation or truncated basis approximation), *J*-shifting is the most severe approximation. Meijer and Goldfield assumed that Coriolis coupling is not important, that the total angular momentum *J* has no impact on the dynamics of the reaction other than introducing a ccentrifugal barrier, and finally, that the centrifugal barrier can be approximated by its value at the transition state. With theses assumptions, Meijer and Goldfield observed significant deviations from the reaction probabilities determined with rigorous close coupling calculations on the DMBE IV PES. Consequently, the approximate cross sections determined by *J*-shifting do not agree very well with the close coupling cross sections.

In late 2000, a new ab initio PES for reaction 1 was developed and utilized by Harding et al.[134,135] and by Troe and Ushakov[136] in both statistical adiabatic channel model (SACM) and quasiclassical trajectory (QCT) calculations of specific ($k(E,J)$) and thermal ($k(T)$) rate coefficients for reaction 1 between 300 and 5000 K. Good agreement with experimental measurements was observed; there was no evidence of nonstatistical effects or contributions from electronically excited states. Below 300 K, QCT treatments were inadequate and only a quantum SACM methodology gave reliable results. Troe and Ushakov noted that utilizing the recently revised[137] value of the OH enthalpy of formation brings the agreement between theory and experiment to within 20% over the temperature range of 300 to 5000 K. Sultanov and Balakrishnan[138] report very recent quantum scattering calculations for reaction 1 using both the DMBE IV PES and the recently developed PES of Harding, Troe, and Ushakov. Using a *J*-shifting approximation, they report that the rate coefficients computed using the Harding, Troe, and Ushakov PES are approximately 50% larger than those computed on the DMBE IV PES. Further, above 1000 K the *J*-shifting approximation appears to be an adequate computational approach for reaction 1, with the Harding, Troe, and Ushakov PES yielding better agreement with experimentally measured rate coefficients than does the DMBE IV PES.

In his review of the history of calculating the forward and reverse rate coefficients for reaction 1, Troe[139] notes that the agreement between theory and experiment over the temperature range from 1000 to 3000 K is approximately ±10%. Further improvement in the determination of rate coefficients for reaction 1 will require more precise thermochemical data and a detailed analysis of the contributions to the rate coefficient from all the electronic states generated by the four open electronic shell species involved in reaction 1.

In this paper we examine the effects of reagent vibrational excitation on the rate coefficients characterizing reaction 1. Calculations have been completed at four different translational temperatures (T = 1000, 2000, 3000, and 4000 K), for five different vibrational excitations of the O_2 reagent (v = 6, 7, 8, 9, 10) on two different analytical PESs, the Melius−Blint[75] (MB) PES and the Pastrana et al. Double Many-Body Expansion[82] (DMBE) IV PES. Both the MB PES and the DMBE IV PES are representations of the ground electronic state (X^2A'') of reaction 1. These surfaces were chosen because the MB PES is the earliest model PES of reaction 1 based on high-quality ab initio data while the DMBE IV PES has been the most widely used realistic PES to study reaction 1. Dating from 1979, the MB PES is based on more than 400 Multi-Configuration Self-Consistent Field (MCSCF) calculations. It has been used over the past twenty-five years in both quasiclassical and quantum mechanical studies of both directions of reaction 1. The DMBE IV PES is a semiempirical PES, using two-body and three-body expansions to represent intramolecular forces and including available experimental and ab initio information. First published in 1990 as a revision of earlier DMBE PESs, the DMBE IV PES has also been used in numerous studies of both the forward and reverse directions of reaction 1. Since the MB PES has been used over a long period, its inclusion in this study provides an important point of reference for a qualitative understanding the effect of reagent vibrational excitation on rate coefficient characterizing reaction 1. Further, because we have chosen to study two different PESs, it will be possible to make a direct comparison of the rate coefficients calculated with the two PESs, noting differences and similarities. Finally, both the MB PES and the DMBE IV PESs are significant improvements over a LEPS PES used by Gauss[88] in an earlier quasiclassical trajectory study of reaction 1 with O_2 vibrationally excited to levels v = 4, 5, 6.

However, both the MB PES and the DMBE IV PES have known deficiencies and we will return to this point later in this paper. Consequently, it is not the goal of this initial study to achieve quantitative agreement with experimental data. Rather, the two PESs are used here in an attempt to provide an initial qualitative understanding of reagent vibrational effects. There are, in fact, several additional PESs, developed after the MB PES and the DMBE IV PES, that have not been as widely used to study reaction 1. In particular, we note the DIM model of Kendrick and Pack[115] (1994), the recent work of Harding et al.[134,135] (2000−2001), and the global PES utilized by Troe and Ushakov[136] (2001). Finally, a new global analytic representation of the PES for reaction 1 utilizing the calculations of both Walch et al.[77−79] and Harding et al.[134,135] is under development in this author's (R.J.D.) laboratory.

Since this study focuses on the effects of reagent vibrational excitation, we examine only a nonrotating O_2 diatom (J = 0). The averaging of trajectory calculations over a distribution of J values presents no theoretical difficulty. However, we have chosen to focus on J = 0 in an attempt to identify any unusual characteristics attributable specifically to the vibrational excitation of the reagents in reaction 1 even though this choice will make a direct comparison with experimentally measured rate coefficients impossible.

The temperature range chosen for this study is consistent with the experimental work of Du and Hessler,[68] who have recommend a rate coefficient for the forward direction of reaction 1 of $k_1(T) = [(1.62 \pm 0.12) \times 10^{-10}]\exp[-(7474 \pm 122)/T(\mathrm{K})]$ $\mathrm{cm^3\ molecule^{-1}\ s^{-1}}$ for a temperature range from 960 to 5300 K. While the calculations completed in this study do not include the highest temperature examined in the work by Du and Hessler, they do cover a sufficiently broad range to demonstrate the qualitative effect of reagent vibrational excitation on the rate coefficient characterizing reaction 1 and to encompass a significant portion of the temperature span accessible to experimental measurements. Using their recently developed theoretical model, Troe and Ushakov[136] recommend a rate coefficient for the reverse direction of reaction 1 in the temperature range 300 K to 5 000 K of $k_{-1}(\mathrm{T}) = (0.026 \times 10^{-10}) \times (\mathrm{T/1\ 000\ K})^{1.47} + (1.92 \times 10^{-10}) \times (\mathrm{T/1\ 000\ K})^{0.46}$ $\mathrm{cm^3\ molecule^{-1}\ s^{-1}}$. Very recent theoretical work[12] has investigated the characteristics of reaction 1 up to a temperature of 10 000 K on the DMBE IV PES.

The paper is organized as follows: In Section II we briefly outline the basic kinetic theory and computational assumptions used in this work. In Section III we summarize the results of these calculations while a discussion and interpretation of these results is presented in Section IV. A summary is given in Section V. In addition to the kinetics and dynamical interpretations presented here, this work is significant in that it is, to the best of our knowledge, the first use of a new Potential Energy Library, POTLIB 2001,[140] to study a reactive chemical system.

II. Computational Methods

The expression defining the thermal rate coefficient $k(T)$ at temperature T for the forward direction of reaction 1, producing the OH diatom and O-atom products, is given by:

$$k(T) = \frac{1}{3}\left(\frac{8kT}{\pi\mu_{\mathrm{H-O_2}}}\right)^{1/2} \sigma^{\mathrm{r}}(T) \qquad (2)$$

In the above equation, $\mu_{\mathrm{H-O_2}}$ is the atom−diatom reduced mass, k is the Boltzmann constant, and the factor of $^1/_3$ accounts for the electronic degeneracy of reaction 1, representing the probability of reaction 1 occurring on the ground-state PES of the HO_2 radical. The standard options of the VENUS96[141] quasiclassical trajectory program were used to select the initial conditions. The vibrational quantum number of the nonrotating O_2 diatom was successively chosen as v = 6, 7, 8, 9, 10, and for each vibrational quantum number of the O_2 diatom, the vibrational energies are chosen by a semiclassical Einstein−Brillouin−Keller (EBK) quantization. An ensemble of 5000 trajectories was computed for each O_2 vibrational quantum number at four different translational temperatures, T = 1000, 2000, 3000, and 4000 K (a total of 100 000 trajectories on each PES). The classical equations of motion were integrated by using a fixed-step integrator (step size = 1×10^{-16} s) that combines fourth-order Runge−Kutta and sixth-order Adams−Moulton algorithms.

The maximum value of the impact parameter, $b_{\max}$, was computed for each temperature and vibrational quantum number combination by computing batches of 1000 trajectories at fixed values of b, systematically increasing the size of b until no reactions were observed in the batch of 1000 trajectories. After $b_{\max}$ was determined for each combination of vibrational

quantum number and translational temperature, the impact parameter for each trajectory in the ensemble of 5000 trajectories for a specified vibrational quantum number and translational temperature was chosen by using a uniformly distributed random number, R, in the interval (0−1):

$$b = b_{\max} R^{1/2} \tag{3}$$

At each temperature, we define the reactive cross section by

$$\sigma^{r}(T) = \pi b_{\max}{}^{2}\left(\frac{N^{r}}{N}\right) \tag{4}$$

where N^r/N is the ratio of the number of reactive trajectories and the total number of trajectories. The 68% confidence level is then calculated by:

$$\Delta\sigma^{r}(T) = \left(\frac{N - N^{r}}{NN^{r}}\right)^{1/2}\sigma^{r}(T) \tag{5}$$

The Cartesian coordinates and velocities of each reactant are randomly oriented through Euler's angles within the reactants' space-fixed center-of-mass Cartesian frame:

$$x_i = R(\vartheta,\phi,\chi)x_{i,\mathrm{cm}} \tag{6a}$$

$$\dot{x}_i = R(\vartheta,\phi,\chi)\dot{x}_{i,\mathrm{cm}} \tag{6b}$$

where the angles θ, ϕ, and χ are chosen by using three random numbers, R_1, R_2, and R_3. A different set of random numbers is used for each reactant.

$$\cos\vartheta = 2R_1 - 1 \tag{7a}$$

$$\phi = 2\pi R_2 \tag{7b}$$

$$\chi = 2\pi R_3 \tag{7c}$$

The relative translational energy, E_{tr}, at each temperature, T, is chosen by using the following probability distribution:[106]

$$P(E_{\mathrm{tr}})\,\mathrm{d}E_{\mathrm{tr}} = \frac{E_{\mathrm{tr}}}{(kT)^2}\exp\left(\frac{-E_{\mathrm{tr}}}{kT}\right)\mathrm{d}E_{\mathrm{tr}} \tag{8}$$

A more detailed account of the Monte Carlo quasiclassical trajectory method can be found in ref 106.

To apply eq 2 to calculate the thermal rate coefficient for each T requires the unambiguous determination of the number of reactive trajectories, N^r. This determination is directly connected with the question of how to treat vibrational zero-point energy (ZPE) in the realm of classical mechanics. While this question has been the subject of many investigations[142−157] and several distinct methodologies[142−147,150,152,154,155] have been proposed, no completely satisfactory computational procedure has emerged.

In this study we have chosen to determine the number of reactive trajectories in two ways. First, we define a reaction to have occurred when the distance between the OH diatom and a single O-atom exceeds 10.0 bohr. This distance is clearly much, much larger than the equilibrium OH bond length and identifies two entirely separate species. However, using such a dynamical definition of a reaction opens the possibility that the resulting OH diatom fragment may contain less than the vibrational ZPE. Consequently, we have chosen to count reactive trajectories a second way by imposing an additional quantum mechanical constraint and requiring the resulting OH diatom to possess at least vibrational ZPE. Under the second protocol, any trajectory that satisfies the dynamical constraint of a separation between the OH diatom and the O-atom, but does NOT satisfy the ZPE constraint is discarded. This is not wholly satisfactory since the ratio N^r/N still utilizes the same denominator (5000 trajectories) thereby altering the probabilities.

We will use these two counting methods as upper and lower bounds on the calculation of thermal rate coefficients, recognizing that neither simple method should be expected to represent the experimental behavior of reaction 1. This is consistent with our interest to observe the qualitative effect of vibrational excitation of the O_2 reagent on the rate coefficients of reaction 1, and not to predict accurately the experimental reaction rate. To determine the value of N^r, we have chosen to use the same estimate of the harmonic OH vibrational ZPE for both the MB PES and the DMBE IV PES. This value, 22.51 kJ mol^{-1} (5.381 kcal mol^{-1}), was calculated by Walch and Duchovic[79] at the Complete Active Space Self-Consistent Field/Contracted Configuration Interaction including the Davidson Correction (CASSCF/CCI+Q) level of theory with a large basis set. The corresponding harmonic OH vibrational frequency is 3764 cm^{-1}. It should be noted that the value of the harmonic OH vibrational ZPE used in this study to determine N^r differs from the anharmonic values on both surfaces by a maximum of 0.410 kJ mol^{-1} (0.1 kcal mol^{-1}). Consequently, the use of this single estimate of the OH vibrational ZPE is not significantly different from using PES-specific values for the OH vibrational ZPE to determine N^r. Further, since the harmonic ZPE value is the largest of the three estimates of the OH vibrational ZPE, its use represents the most conservative determination of N^r.

TABLE 1: Potential Energy Surface Characteristics: Stationary Points, Energies, and Excited-State O_2 Vibrational Energies

	$H + O_2$	$H-O_2$ saddle	HO_2	$OH-O$ saddle	$OH + O$
		Melius−Blint PES			
r_{OH}		3.76	1.88		1.85
r_{OO}	2.32	2.33	2.58		
θ		120	104		
energy	0.00	1×10^{1}	−250		58
		DMBE IV PES			
r_{OH}		7.547	1.8345	1.820	1.835
r_{OO}	2.283	2.282	2.5143	5.083	−
θ		180.0	104.29	40.2	−
energy	0.00	7.876×10^{-2}	−229.5	49.28	56.11

	O_2 vibrational energy (kJ mol^{-1})			
	Melius−Blint PES		DMBE IV PES	
quantum no.	Harmonic	EBK[b]	Harmonic	EBK[b]
6	123.9	115.7	122.6	117.5
7	142.9	132.0	141.5	134.6
8	162.0	147.9	160.3	151.4
9	181.0	163.5	179.2	167.9
10	200.1	178.7	198.0	184.2

[a] Distances are measured in bohr and angles in degrees. PES energies are reported in kJ mol^{-1} relative to the $H + O_2$ asymptote. [b] Einstein−Brillouin−Keller semiclassical quantization used to determine vibrational energies. O_2 ground-state harmonic frequencies: 1593.0 cm^{-1} (Melius−Blint); 1576.7 cm^{-1} (DMBE IV).

III. Results

A. Vibrational Excitation. To orient the reader to characteristics of the MB PES and the DMBE IV PES, the upper portion of Table 1 summarizes the key features of each PES. As the table indicates, reaction 1 is endothermic in the forward

TABLE 2: Rate Coefficients[a] for the Reaction H + O_2 → OH + O at Four Temperatures as a Function of O_2 Vibrational Quantum Number

temp (K)	$v = 6$	$v = 7$	$v = 8$	$v = 9$	$v = 10$
			Melius−Blint PES		
1000.0	−11.65	−11.41	−11.11	−11.03	−10.93
2000.0	−11.39	−11.15	−11.00	−10.94	−10.87
3000.0	−11.27	−11.03	−10.94	−10.87	−10.81
4000.0	−11.10	−10.98	−10.88	−10.77	−10.71
			DMBE IV PES		
1000.0	−11.81	−11.61	−11.49	−11.27	−11.20
2000.0	−11.58	−11.46	−11.32	−11.25	−11.03
3000.0	−11.51	−11.35	−11.14	−11.08	−11.02
4000.0	−11.34	−11.20	−11.16	−11.05	−11.03
			Melius−Blint PES, no ZPE constraint		
1000.0	−11.33	−11.23	−11.01	−10.95	−10.88
2000.0	−11.16	−11.01	−10.91	−10.86	−10.80
3000.0	−11.09	−10.90	−10.85	−10.81	−10.73
4000.0	−10.96	−10.88	−10.78	−10.71	−10.65
			DMBE IV pes, no ZPE constraint		
1000.0	−11.50	−11.39	−11.30	−11.16	−11.09
2000.0	−11.34	−11.30	−11.21	−11.16	−10.93
3000.0	−11.28	−11.19	−11.04	−10.99	−10.94
4000.0	−11.17	−11.11	−11.04	−10.97	−10.94

[a] Log of the rate coefficients in units of cm^3 $molecule^{-1}$ s^{-1} are reported.

direction by 58 kJ mol^{-1} on the MB PES and by 56.11 kJ mol^{-1} on the DMBE IV PES. Both PESs identify the HO_2 as a bent species, with the HOO angle being 104.2° on the MB PES and 104.29° on the DMBE IV PES. The MB PES possesses a barrier in the entrance channel of 10 kJ mol^{-1} compared to a barrier of less than 0.1 kJ mol^{-1} on the DMBE IV PES. Finally, the reader will note that in the OH + O exit channel the OH bond length remains virtually unchanged on both PESs. In the lower portion of Table 1 we summarize the O_2 reactant energies as a function of vibrational quantum number. As noted in the discussion above, the O_2 vibrational energy on each surface was chosen by using a semiclassical EBK quantization procedure. The table demonstrates that there is a significant difference between the energy based on the harmonic ground-state frequency and the vibrational energies derived from the EBK quantization procedure. This difference is a reflection of the anharmonicity of each surface at higher levels of vibrational excitation and this anharmonicity must be represented in the choice of initial conditions. Table 1 also contains the ground-state O_2 harmonic frequency on each surface (based on a normal-mode analysis with each PES).

The rate coefficients characterizing reaction 1 at four different temperatures as a function of O_2 vibrational quantum number are summarized in Table 2 for each PES. The table contains two sets of data for each PES, one in which no ZPE constraint has been imposed (relying on the simple dynamical definition of a reaction given above), and a second set in which a minimum vibrational ZPE is required for each OH product. Each temperature−vibrational quantum number value in the table is the result of an ensemble of 5000 trajectories calculated after a specific b_{max} was chosen (as described above) for each combination of temperature and vibrational quantum number. The data reported in Table 2 required a total of 319 000 trajectory calculations (rate coefficient calculations and b_{max} determinations for each temperature−quantum number combination).

The table demonstrates several clear trends in the data. For each temperature, on both PESs with and without the imposition of the ZPE constraint, the rate coefficient increases monotonically with O_2 vibrational quantum number. This observation is consistent both with the trend observed in an earlier study by Teitelbaum and Lifshitz,[158] which used a nonequilibrium kinetics model, and with the trend reported in a very recent work by Teitelbaum et al.,[12] which has explored O_2 vibrational quantum numbers $v = 0$ to 15 and temperatures up to 10 000 K. At the 68% confidence level (eq 5), the rate coefficients calculated with the ZPE constraint are statistically different from those calculated without the imposition of the ZPE constraint. This occurs on both PESs used in this study. Examining only those trajectories satisfying the ZPE constraint on the MB PES at $T = 1000$ K, the total rate coefficient for increases by a factor of 5.2 as the initial vibrational quantum number of the O_2 diatom increases from $v = 6$ to 10. For $T = 2000$ K, this factor drops to 3.3, to 2.9 for $T = 3000$ K, and to 2.5 for $T = 4000$ K (see Table 2). On the DMBE IV PES the total rate coefficient (for ZPE constrained trajectories) increases by a factor of 4.1 as the initial vibrational quantum number of the O_2 diatom increases from $v = 6$ to 10 for $T = 1000$ K. For $T = 2000$ K this factor drops to 3.5, to 2.1 for $T = 3000$ K, and to 2.0 for $T = 4000$ K (see Table 2). On both PESs, with and without the imposition of the ZPE constraint, an analysis of the data for each quantum number reveals that the rate coefficient increases nearly monotonically as a function of temperature. On the DMBE IV PES, the departures from a strictly monotonic increase are not statistically significant at the 68% confidence level (eq 5).

B. Reactive Cross Sections. Table 3 reports reactive cross sections (in Å^2) calculated on the MB PES and the DMBE IV PES as a function of the relative translational energy of the reactants in the forward direction of reaction 1. Trajectories were binned in increments of 20.92 kJ mol^{-1} (5.00 kcal mol^{-1}) and the average relative translational energy was calculated for each bin. As with the experimental data of Bajeh et al.,[131] the calculations with $v \neq 0$ in Table 3 do not exhibit the relatively sharp increase in reactivity between 115.8 (1.2 eV mol^{-1}) and 164.0 kJ mol^{-1} (1.7 eV mol^{-1}) observed in earlier experimental studies.[50,52,53] This same sharp increase was also absent from the quantum mechanical ($v = 0$) calculations of Meijer and Goldfield.[128−130,133]

The data in Table 3 demonstrate a nearly monotonic decrease (with only a limited number of exceptions) in the reactive cross sections as a function of energy. This monotonicity is exhibited both in the averaging of the cross sections over temperature and in averaging the cross sections over the O_2 vibrational quantum number. It is interesting to note that this behavior occurs on both PESs utilized in this study.

Table 4 reports the calculated reactive cross sections (in Å^2) as a function of the number of trajectory time steps (time step $= 1 \times 10^{-16}$ s). The trajectories were binned every 500 time steps on the MB PES and every 1000 time steps on the DMBE IV PES. The different bin sizes demonstrate that the observed qualitative behavior remains the same even though the courseness of the binning procedure is varied. As in Table 3, the average relative translational energy was calculated for each bin. As a function of the number of trajectory time steps (i.e. time), the reactive cross sections increase monotonically on both PESs, approaching asymptotic values. The asymptotic values, as a function of O_2 vibrational quantum number (averaged over temperature), span a greater range than those reported as a function of temperature (averaged over O_2 vibrational quantum number). This behavior occurs on both PESs; however, the asymptotic values of the reactive cross sections also differ significantly on the two PESs.

Additionally, the data of Table 4 indicate that the rate at which the reactive cross section increases as a function of trajectory time step declines as the total time of the trajectories increases. We define a cross-section factor as the ratio cs_{n+1}/cs_n where

TABLE 3: Reactive Cross Section[a]

energy[b]	av energy[c]	$v = 6$	$v = 7$	$v = 8$	$v = 9$	$v = 10$	1000 K	2000 K	3000 K	4000 K
					Melius−Blint PES					
20.92	12.00	0.186	0.364	0.603	0.802	0.981	1.24	0.572	0.337	0.198
41.84	30.09	0.187	0.295	0.468	0.563	0.613	0.317	0.550	0.461	0.373
62.76	51.55	0.0984	0.175	0.250	0.229	0.314	0.0429	0.224	0.283	0.302
83.68	72.04	0.0981	0.133	0.143	0.190	0.223		0.0876	0.173	0.212
104.60	92.52	0.0863	0.112	0.0865	0.105	0.0919		0.0311	0.0888	0.169
125.52	114.44	0.0428	0.0495	0.0591	0.0750	0.0673		0.0221	0.0534	0.101
146.44	135.78	0.0565	0.0412	0.0383	0.0744	0.0672		0.00862	0.0412	0.0941
167.36	157.01	0.0315	0.0329	0.0347	0.0547	0.03931			0.0188	0.0513
188.28	177.63	0.0181	0.0211	0.0202	0.0274	0.0101			0.0110	0.0224
209.20	198.41	0.00511	0.0158	0.0170	0.0175	0.0635		0.00770	0.00493	0.0258
230.12	218.47	0.00757	0.00528		0.0137				0.00985	0.00808
251.04	239.16	0.00528				0.0132		0.00814		0.00957
271.96	265.39			0.00565						0.00565
292.88	292.55			0.00565						0.00565
					DMBE IV PES					
20.92	11.99	0.112	0.190	0.297	0.440	0.545	0.621	0.331	0.214	0.101
41.84	30.51	0.110	0.162	0.207	0.294	0.365	0.215	0.279	0.263	0.155
62.76	51.67	0.0875	0.0988	0.113	0.115	0.155	0.0400	0.128	0.122	0.140
83.68	72.48	0.0701	0.0990	0.0851	0.138	0.154	0.00860	0.0747	0.128	0.140
104.60	92.54	0.0387	0.0506	0.0672	0.0674	0.0791	0.00458	0.0276	0.0742	0.0869
125.52	115.24	0.0268	0.0276	0.0503	0.0544	0.0697		0.00985	0.0276	0.0674
146.44	134.77	0.0354	0.0361	0.0400	0.0333	0.0481		0.0111	0.0266	0.0579
167.36	156.43	0.0137	0.0234	0.0270	0.0272	0.0146		0.0111	0.0154	0.0278
188.28	178.63	0.00785	0.0127	0.0137	0.0181	0.0121			0.0122	0.0129
209.20	200.84	0.00785	0.00425	0.00643	0.0121	0.0121			0.00643	0.00907
230.12	222.90	0.00393	0.00425		0.00604					0.00474
251.04	238.93	0.00785				0.0121				0.00997
271.96	259.09	0.00393			0.0121	0.0121				0.00936
292.88	289.22			0.00684		0.00604				0.00644
313.80	304.47		0.00849							0.00849
334.72										
355.64	350.79					0.00604				0.00604

[a] The table reports average cross sections. The first five columns are cross sections for each quantum number averaged over the four temperatures used in this study. The last four columns are cross sections for each temperature averaged over the five values of the O_2 vibrational quantum number used in this study. Energies are reported in kJ mol^{-1} and cross sections are reported in Å^2. [b] Trajectories were binned based on the initial translational energy of the H + O_2 reactants in increments of 20.92 kJ mol^{-1} (5.00 kcal mol^{-1}). [c] Average initial translational energy of the H + O_2 reactants for all trajectories in each energy bin.

cs_{n+1} is the cross section of the $(n + 1)$th bin and cs_n is the cross section of the nth bin. With use of Table 4, the data from the MB PES indicate that the reactive cross sections calculated at 4000 time steps are smaller by factors that range from 3.12 (1000 K) to 1.35 (4000 K) than the reactive cross sections calculated at 5000 time steps. The corresponding factors for the increase in the reactive cross sections at 6000 time steps compared with those at 5000 time steps are 1.50 (1000 K) to 1.18 (4000 K). The significant point of this analysis is that the largest factors occur at the transition from 4000 time steps to 5000 time steps, *suggesting* that there are two groups of trajectories which behave differently.

The same analysis was carried out on the DMBE IV PES starting at 4500 time steps. Averaging over the O_2 vibrational quantum number, the reactive cross sections calculated at 4500 time steps are smaller by factors that range from 2.10 (1000 K) to 1.35 (4000 K) than the reactive cross sections calculated at 5500 time steps. The corresponding factors for the increase in the reactive cross sections at 6500 time steps compared with those at 5500 time steps are 1.39 (1000 K) to 1.16 (4000 K), and the factors for the increase in the reactive cross sections at 7500 time steps compared with those at 6500 time steps are 1.22 (1000 K) to 1.08 (4000 K). Again, the significant point of this analysis is that the largest factors occur at the transition from 4500 time steps to 5500 time steps, *suggesting* that there are two groups of trajectories which behave differently on the DMBE IV PES.

An alternative analysis can be made by calculating all the individual cross-section factors. For each time step bin there are a total of 20 such cross-section factors, one for each quantum number and temperature combination. Averaging these 20 factors for each time step bin yields average cross-section factors which vary from 2.71 (transition from 3000 time steps to 3500 time steps) to 1.01 (transition from 11 000 time steps to 11 500 time steps) on the MB PES. On the DMBE IV PES, the average cross-section factors vary from 8.65 (transition from 3000 time steps to 3500 time steps) to 1.03 (transition from 12 000 time steps to 12 500 time steps). This variation in cross-section factors is displayed graphically in Figure 1.

The cross-section factors are a measure of how rapidly the reactive cross section changes in increments of 500 time steps on the MB PES and in increments of 1000 time steps on the DMBE IV PES. For reactive trajectories on the MB PES that last between 3500 and 5000 time steps, the reactive cross sections increase in size by factors that are significantly greater than 1.00. On the DMBE IV PES, the reactive cross sections of trajectories lasting between 4000 and 5500 time steps increase in size by factors that are also significantly greater than 1.00. These observations indicate that the rate-of-change of the size of the reactive cross sections changes dramatically for reactive trajectories lasting between 3500 time steps and 5500 time steps compared to reactive trajectories lasting for times greater than 5500 time steps.

Insufficient data exist to identify a sharp demarcation in dynamical behavior. In fact, it may be the case that the change in behavior does extend over a period of time. However, the two curves in Figure 1 *suggest* that the qualitative microscopic dynamics of reaction 1 change at approximately 4000 time steps on the MB PES and at approximately 4500 time steps on the DMBE IV PES. This observation led to a subsequent analysis

TABLE 4: Reactive Cross Sections[a]

time[b] steps	av energy[c]	$v = 6$	$v = 7$	$v = 8$	$v = 9$	$v = 10$	1000 K	2000 K	3000 K	4000 K
					Melius−Blint					
3500	55.30	0.120	0.192	0.307	0.482	0.634	0.0933	0.282	0.414	0.599
4000	47.76	0.178	0.308	0.489	0.757	0.954	0.207	0.495	0.611	0.835
4500	40.62	0.243	0.425	0.699	0.995	1.28	0.443	0.673	0.781	1.01
5000	35.44	0.319	0.561	0.853	1.19	1.49	0.646	0.841	0.914	1.13
5500	35.70	0.394	0.652	1.01	1.37	1.68	0.852	0.960	1.03	1.24
6000	32.94	0.444	0.728	1.13	1.47	1.83	0.967	1.07	1.13	1.33
6500	29.55	0.490	0.791	1.22	1.57	1.90	1.06	1.15	1.19	1.37
7000	29.10	0.530	0.840	1.29	1.63	1.98	1.17	1.20	1.25	1.40
7500	30.36	0.563	0.885	1.32	1.68	2.02	1.22	1.25	1.29	1.43
8000	31.40	0.585	0.905	1.37	1.74	2.06	1.28	1.28	1.32	1.45
8500	30.94	0.602	0.930	1.40	1.77	2.09	1.34	1.31	1.33	1.46
9000	27.21	0.618	0.958	1.44	1.80	2.14	1.40	1.34	1.36	1.48
9500	28.14	0.630	0.980	1.46	1.83	2.16	1.42	1.37	1.37	1.48
10000	28.32	0.640	0.997	1.49	1.85	2.17	1.45	1.39	1.38	1.50
10500	30.27	0.652	1.01	1.50	1.86	2.19	1.46	1.41	1.39	1.51
11000	31.90	0.660	1.03	1.51	1.86	2.22	1.48	1.42	1.40	1.52
11500	26.53	0.668	1.04	1.52	1.88	2.22	1.50	1.43	1.41	1.52
					DMBE IV					
3500	69.05	0.0671	0.0901	0.186	0.206	0.248	0.0858	0.122	0.193	0.220
4500	48.54	0.126	0.209	0.280	0.419	0.527	0.176	0.259	0.394	0.419
5500	37.81	0.190	0.298	0.442	0.641	0.781	0.369	0.423	0.522	0.567
6500	36.53	0.256	0.397	0.561	0.801	0.949	0.512	0.570	0.630	0.659
7500	33.56	0.305	0.467	0.637	0.897	1.06	0.624	0.658	0.698	0.714
8500	29.01	0.334	0.509	0.683	0.948	1.13	0.689	0.700	0.754	0.743
9500	29.68	0.362	0.536	0.725	0.981	1.18	0.739	0.744	0.789	0.757
10500	37.37	0.372	0.560	0.742	1.01	1.22	0.781	0.772	0.802	0.768
11500	37.46	0.385	0.574	0.759	1.03	1.24	0.802	0.788	0.819	0.779
12500	28.67	0.390	0.584	0.783	1.04	1.28	0.82	0.811	0.838	0.789

[a] The table reports average cross sections. The first five columns are cross sections for each quantum number averaged over the four temperatures used in this study. The last four columns are cross sections for each temperature averaged over the five values of the O_2 vibrational quantum number used in this study. Energies are reported in kJ mol^{-1} and cross sections are reported in $Å^2$. [b] Trajectories were binned as a function of the length of a trajectory (i.e., the number of time steps). The length of a time step is 1.0×10^{-16} s. [c] Average initial translational energy of the H + O_2 reactants for all trajectories in each energy bin.

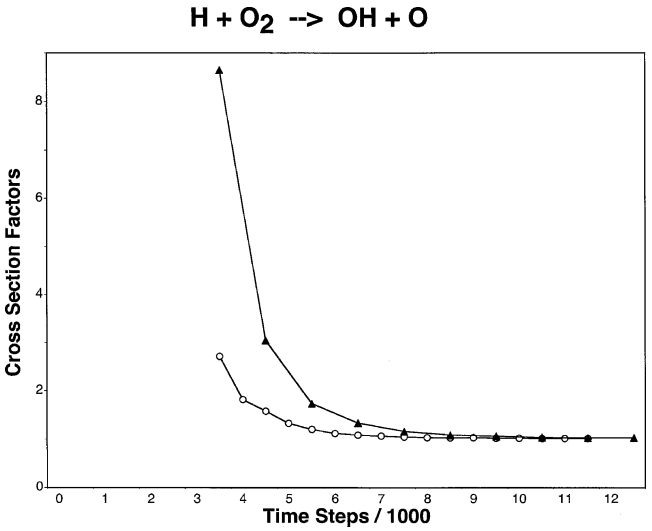

Figure 1. Cross-section factors (see text) averaged over both temperature and O_2 vibrational quantum number: (○) average cross-section factors calculated on the MB PES; (▲) average cross-section factors calculated on the DMBE IV PES.

(reported below) that examines the effect of O_2 reagent vibrational excitation on the rate of reaction 1. We call those trajectories which react in 4000 time steps or less on the MB PES or 4500 time steps or less on the DMBE IV PES "more-direct" trajectories. Trajectories which react in more than 4000 time steps on the MB PES or more than 4500 time steps on the DMBE IV PES are called "less-direct" trajectories.

The data contained in Table 5 are a summary of the individual trajectory calculations. For each temperature−quantum number combination on each PES, a quartet of values is reported. The first line of data at each temperature records the number of reactive trajectories that satisfied both the dynamical reaction definition and the ZPE constraint applied to the OH product. The second line of data reports the number of trajectories forming OH + O products based solely on the dynamical reaction definition. For each quantum number, the first of the two values is the number of more-direct trajectories. The second of the two values is the number of less-direct trajectories.

The identification of two groups of trajectories on each PES is further supported by a simple analysis of the average number of turning points for each group of trajectories. A trajectory "turning point" was identified by monitoring the sign of the momentum vector associated with the center-of-mass of the reacting system. Each time this vector changed its sign, a turning point was counted. This analysis indicates that there is a distinct difference in dynamical behavior between the two groups of trajectories. In Table 6 we report the average number of turning points at each temperature−quantum number combination for those reactive trajectories forming products and satisfying the ZPE constraint for the OH diatom on the MB PES and on the DMBE IV PES. Noting that the less-direct group of trajectories executes, on average, nearly twice as many turning points as the more-direct group of trajectories supports the identification of the different dynamical behavior exhibited by the two groups on each PES. It is important to note that the observed disparity in the number of turning points was not used as the criterion for identifying the two apparent groups of trajectories. In fact, the available data do not provide information about the location of the turning points, that is, are they occurring in the vicinity of the deep potential energy well of reaction 1 or are they

TABLE 5: Number of Reactive Trajectories as a Function of Temperature and O_2 Vibrational Quantum Number (v)

	$v = 6$		$v = 7$		$v = 8$		$v = 9$		$v = 10$	
temp[c] (K)	more direct[a]	less direct[b]	more direct[a]	less direct[b]	more direct[a]	less direct[b]	more direct[a]	less direct[b]	more direct[a]	less direct[b]
					Melius−Blint PES					
1000	3	88	10	99	16	144	23	99	18	118
	10	180	17	151	25	179	25	120	23	131
2000	18	108	47	143	84	201	91	151	113	156
	32	181	62	202	108	249	111	181	136	182
3000	41	104	66	125	94	156	94	128	99	86
	58	163	85	173	123	189	105	150	123	101
4000	75	98	84	142	130	136	169	115	159	89
					DMBE IV PES					
1000	4	74	17	76	15	72	18	60	22	71
	17	141	36	120	29	105	32	79	38	81
2000	18	70	31	77	22	79	24	45	50	88
	37	113	48	108	34	97	35	49	65	108
3000	44	60	49	92	62	87	45	47	53	52
	75	102	78	123	82	105	55	56	68	56
4000	57	77	85	86	62	53	87	84	93	85
	95	104	108	103	85	69	108	95	120	99

[a] More-direct trajectories formed O + OH products in 4000 time steps or less on the MB PES and in 4500 time steps or less on the DMBE IV PES. [b] Less-direct trajectories formed O + OH products in more than 4000 time steps or on the MB PES and in more than 4500 time steps on the DMBE IV PES. [c] At each temperature, the first line of data reports the number of trajectories which satisfied both the dynamical definition of a reaction and the ZPE constraint when forming the O + OH products (see text); the second line of data reports the number of trajectories satisfying only the dynamical definition of a reaction when forming the O + OH products (see text).

TABLE 6: Average Number of Turning Points (total) for ZPE-Constrained Reactive Trajectories as a Function of Temperature and O_2 Vibrational Quantum Number (v)

temp (K)		$v = 6$	$v = 7$	$v = 8$	$v = 9$	$v = 10$
			Melius−Blint PES			
1000.0	more direct[a]	33	37	34	35	31
	less direct[b]	68	78	74	62	64
2000.0	more direct[a]	32	32	32	32	28
	less direct[b]	79	79	69	68	65
3000.0	more direct[a]	31	32	31	32	27
	less direct[b]	73	70	74	67	56
4000.0	more direct[a]	32	29	29	28	27
	less direct[b]	70	70	70	59	55
			DMBE IV PES			
1000.0	more direct[a]	28	30	30	33	24
	less direct[b]	71	72	68	59	69
2000.0	more direct[a]	31	33	30	29	29
	less direct[b]	92	70	69	73	65
3000.0	more direct[a]	31	30	32	30	30
	less direct[b]	74	76	71	68	76
4000.0	more direct[a]	29	31	29	28	27
	less direct[b]	84	73	68	72	68

[a] More-direct trajectories formed O + OH products in 4000 time steps or less on the MB PES and in 4500 time steps or less on the DMBE IV PES. [b] Less-direct trajectories formed O + OH products in more than 4000 time steps or on the MB PES and in more than 4500 time steps on the DMBE IV PES.

occurring primarily in the exit channel of reaction 1. The observed disparity in the total number of turning points is simply an indicator that the two groups of trajectories appear to execute different dynamics.

C. Rate Coefficients. To display the effect of the initial vibrational excitation of the O_2 reagent on the rate coefficient of reaction 1, data calculated with the DBME IV PES (Table 2) for those trajectories satisfying the ZPE constraint are plotted in Figure 2 as a function of $E_{tot} = 1.5kT + E_{vib}$, where E_{vib} are the EBK O_2 vibrational energies from Table 1.

The figure shows that initial reagent vibrational excitation, in general, does not increase the total rate coefficient for reaction 1 more than the increase due to a simple temperature increase. The data plotted in Figure 2 indicate that increase in the rate

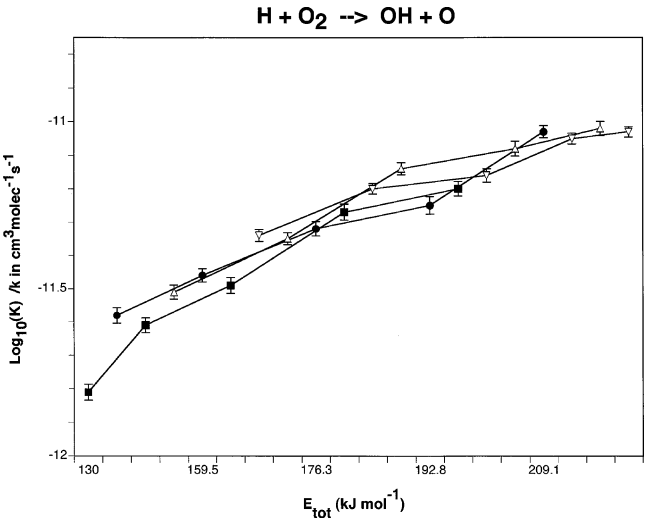

Figure 2. Rate coefficients (k) calculated from reactive trajectories (both less-direct and more-direct) satisfying both the dynamical and the ZPE constraints (see text) on the DMBE IV PES: (■) log(k) calculated at $T = 1000$ K; (●) log(k) calculated at $T = 2000$ K; (△) log(k) calculated at $T = 3000$ K; (▽) log(k) calculated at $T = 4000$ K. The error bars represent the 68% confidence interval.

coefficients is strongly controlled by the simple increase in temperature, with the total rate coefficients calculated for each of the four temperatures and the five O_2 vibrational quantum numbers increasing at very nearly the same rate. This same behavior is observed for the data calculated with the MB PES.

Separating the trajectories into categories of more-direct and less-direct yields a more interesting behavior. In Figure 3, the rate coefficients calculated from the less-direct group of trajectories on the DMBE IV PES are plotted as a function of E_{tot}. The figure indicates that there is a significant enhancement of the rate coefficient of reaction 1 as a result of the initial O_2 vibrational excitation compared to the effect of simple temperature changes. The data in Figure 3 show that the largest rate coefficients are associated with the lowest temperatures and the largest initial O_2 vibrational excitation. Hence, for the less-direct group of trajectories, the initial O_2 vibrational excitation has a

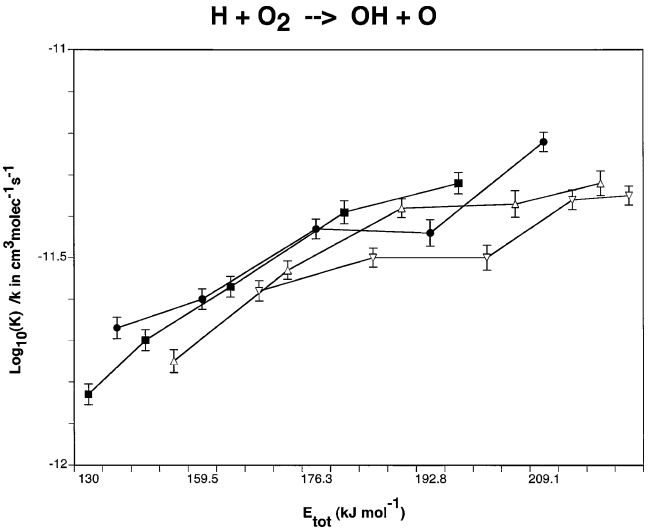

Figure 3. Rate coefficients (k) calculated from the less-direct group of reactive trajectories satisfying both the dynamical and the ZPE constraints (see text) on the DMBE IV PES: (■) log(k) calculated at $T = 1000$ K; (●) log(k) calculated at $T = 2000$ K; (△) log(k) calculated at $T = 3000$ K; (▽) log(k) calculated at $T = 4000$ K. The error bars represent the 68% confidence interval.

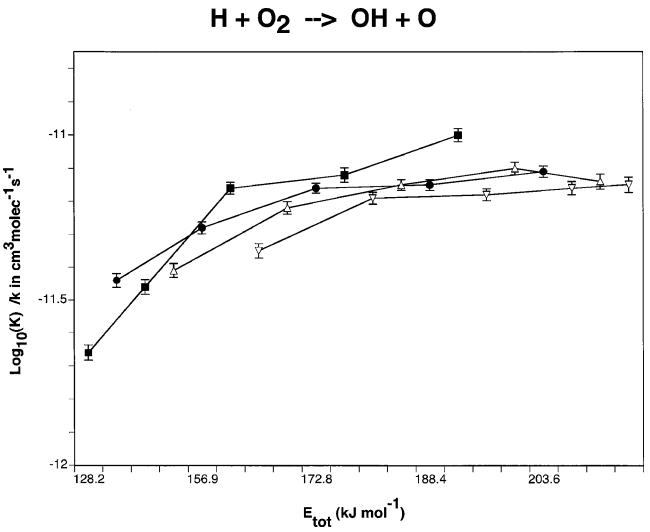

Figure 4. Rate coefficients (k) calculated from the less-direct group of reactive trajectories satisfying both the dynamical and the ZPE constraints (see text) on the MB PES: (■) log(k) calculated at $T = 1000$ K; (●) log(k) calculated at $T = 2000$ K; (△) log(k) calculated at $T = 3000$ K; (▽) log(k) calculated at $T = 4000$ K. The error bars represent the 68% confidence interval.

much greater effect on the rate coefficient of reaction 1 than does the simple increase in temperature. This behavior is also observed on the MB PES (Figure 4).

For the more-direct group of trajectories on both the DMBE IV PES and the MB PES, the rate coefficients for reaction 1 exhibit no significant enhancement due to the initial vibrational excitation of the O_2 reagent compared to the effect of a simple temperature increase. Figure 5 displays the rate coefficients calculated on the MB PES from the more-direct group of trajectories as a function of E_{tot}.

In Figures 6 and 7, the log of the rate coefficient for reaction 1 calculated on the MB PES is plotted as a function of vibrational quantum number for $T = 1000$ K (Figure 6) and 2000 K (Figure 7). Each figure contains four sets of data. The solid symbols depict the rate coefficients calculated for the entire ensemble of 5000 trajectories at each temperature−quantum

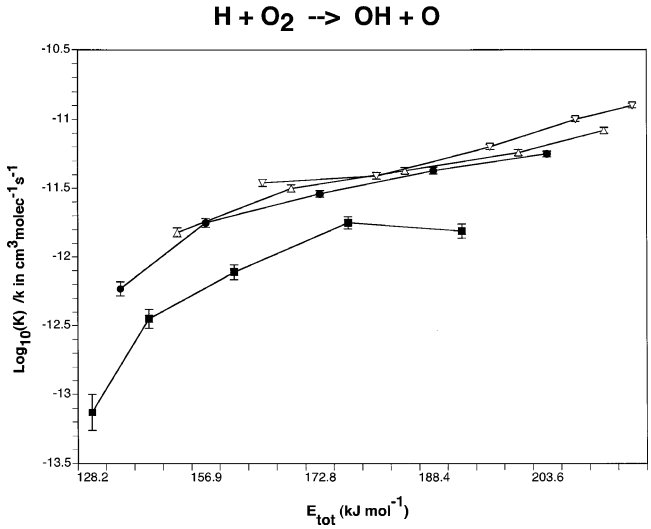

Figure 5. Rate coefficients (k) calculated from the more-direct group of reactive trajectories satisfying both the dynamical and the ZPE constraints (see text) on the MB PES: (■) log(k) calculated at $T = 1000$ K; (●) log(k) calculated at $T = 2000$ K; (△) log(k) calculated at $T = 3000$ K; (▽) log(k) calculated at $T = 4000$ K. The error bars represent the 68% confidence interval.

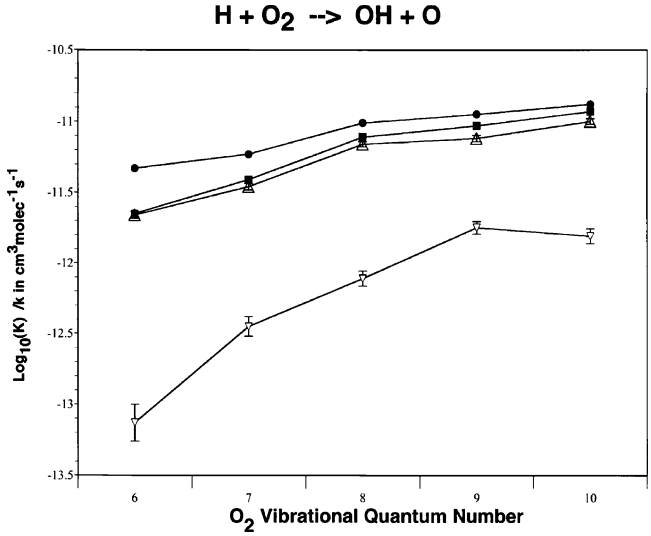

Figure 6. Rate coefficients calculated on the MB PES. Solid symbols are total rate coefficients at $T = 1000$ K: (■) log(k) calculated from reactive trajectories satisfying both the dynamical and the ZPE constraints (see text); (●) log(k) calculated from reactive trajectories satisfying only the dynamical constraint (see text). Open symbols are rate coefficients calculated from more-direct and less-direct trajectories at $T = 1000$ K: (▽) log(k) calculated from more-direct reactive trajectories satisfying both the dynamical and the ZPE constraints (see text); (△) log(k) calculated from less-direct reactive trajectories satisfying both the dynamical and the ZPE constraints (see text). The error bars represent the 68% confidence interval.

number combination. The data represented by the solid circles were calculated by using the trajectories identified as "reactive" based on the dynamical definition of reaction, while the data represented by the solid squares were calculated by using trajectories identified as "reactive" based on the additional requirement that the ZPE constraint be satisfied for the OH diatom product. The data in Figures 6 and 7 show the monotonic behavior for the forward rate coefficient for reaction 1 as noted above. The open symbols in Figures 6 and 7 represent the log of the forward rate coefficient for the more-direct and less-direct groups of trajectories at $T = 1000$ K (Figure 6) and 2000 K (Figure 7). All the trajectories in these two groups satisfy the

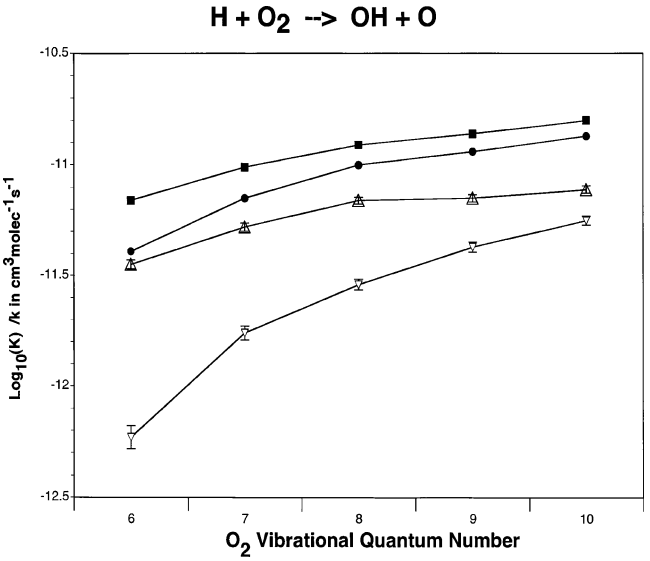

Figure 7. Rate coefficients calculated on the MB PES. Solid symbols are total rate coefficients at $T = 2000$ K: (■) log(k) calculated from reactive trajectories satisfying both the dynamical and the ZPE constraints (see text); (●) log(k) calculated from reactive trajectories satisfying only the dynamical constraint (see text). Open symbols are rate coefficients calculated from more-direct and less-direct trajectories at $T = 2000$ K: (▽) log(k) calculated from more-direct reactive trajectories satisfying both the dynamical and the ZPE constraints (see text); (△) log(k) calculated from less-direct reactive trajectories satisfying both the dynamical and the ZPE constraints (see text). The error bars represent the 68% confidence interval.

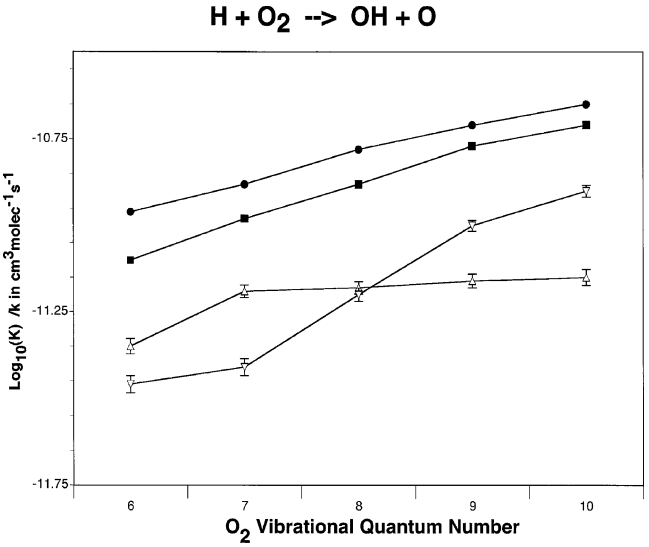

Figure 8. Rate coefficients calculated on the MB PES. Solid symbols are total rate coefficients at $T = 4000$ K: (■) log(k) calculated from reactive trajectories satisfying both the dynamical and the ZPE constraints (see text); (●) log(k) calculated from reactive trajectories satisfying only the dynamical constraint (see text). Open symbols are rate coefficients calculated from more-direct and less-direct trajectories at $T = 4000$ K: (▽) log(k) calculated from more-direct reactive trajectories satisfying both the dynamical and the ZPE constraints (see text); (△) log(k) calculated from less-direct reactive trajectories satisfying both the dynamical and the ZPE constraints (see text). The error bars represent the 68% confidence interval.

ZPE constraint for the OH diatom. The data graphed with the open inverted triangles are computed from the more-direct trajectories while the data represented by the open triangles are computed from the less-direct trajectories (on the MB PES). In both case, the error bars represent the 68% confidence level.

In Figure 6 ($T = 1000$ K), it is clear that the total rate is overwhelmingly determined by the less-direct trajectories for all vibrational quantum numbers 6 through 10. The more-direct trajectories contribute very little to the total rate at this temperature. In Figure 7 ($T = 2000$ K) it is evident that the contribution to the total rate coefficient by the more-direct trajectories becomes more important at the higher vibrational quantum numbers. The data from the DMBE IV PES exhibit the same qualitative behavior for $T = 1000$ and 2000 K. At a temperature of $T = 3000$ K, the behavior of the more-direct and less-direct groups of trajectories on the two PESs begins to diverge. For the MB PES, between $v = 9$ and 10, the relative importance of the more-direct and less-direct trajectories is interchanged, with the more-direct trajectories contributing more substantially to the total rate coefficient of reaction 1. The difference is seen very clearly at $T = 4000$ K. Figure 8 plots the same data as Figures 6 and 7 but at $T = 4000$ K for the MB PES while Figure 9 displays these data for the DMBE IV PES. Again, the error bars represent the 68% confidence level. At $T = 4000$ K on the MB PES (Figure 8), the interchange point between the more-direct and less-direct trajectories occurs at vibrational quantum number $v = 8$. Since the error bars in the data overlap at $v = 8$, the two groups of trajectories at that level of vibrational excitation are making essentially an equal contribution to the total rate coefficient. At $v = 9$ and 10, the more-direct trajectories contribute most significantly to the total rate coefficient for reaction 1. On the DMBE IV PES at $T = 4000$ K (Figure 9), the roles of the more-direct and less-direct trajectories become virtually identical, particularly for $v = 7$, 8, 9, and 10, in contrast to the role reversal observed on the MB PES.

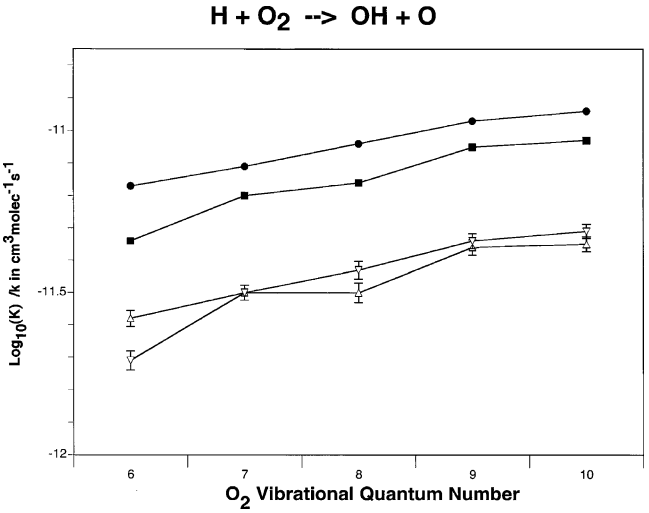

Figure 9. Rate coefficients calculated on the DMBE IV PES. Solid symbols are total rate coefficients at $T = 4000$ K: (■) log(k) calculated from reactive trajectories satisfying both the dynamical and the ZPE constraints (see text); (●) log(k) calculated from reactive trajectories satisfying only the dynamical constraint (see text). Open symbols are rate coefficients calculated from more-direct and less-direct trajectories at $T = 4000$ K: (▽) log(k) calculated from more-direct reactive trajectories satisfying both the dynamical and the ZPE constraints (see text); (△) log(k) calculated from less-direct reactive trajectories satisfying both the dynamical and the ZPE constraints (see text). The error bars represent the 68% confidence interval.

IV. Discussion

The focus of this study on reagent vibrational excitation has yielded an unexpected feature. It appears that contributions to the rate of reaction 1 come from two different trajectory regimes.

The terms "more-direct" and "less-direct" used to describe these two groupings of trajectories reflect that the rate of change of the size of the reactive cross section undergoes a significant change at approximately 4000 time steps on the MB PES and at approximately 4500 time steps on the DMBE IV PES. The identification of two groups of trajectories is further suggested by the gross qualitative difference in the average number of trajectory turning points characterizing these groups (Table 6). With the exception of two cases, the average number of turning points for the less-direct group of trajectories is at least a factor of 2 greater than the average number of turning points for the more-direct group. While this apparent dichotomy was initially determined by an analysis of the reactive cross section, we have also seen that the two groups are further distinguished by the effect of the initial O_2 vibrational excitation on the rate coefficients for reaction 1. Thus, in the study of a single reaction 1 we are able to investigate the effects of reagent vibrational excitation on these two different dynamical regimes. Since the less-direct group of trajectories take a greater number of time steps (i.e. a longer time) to react, it would be expected that these trajectories would yield rate coefficients that are statistical in nature, sensitive only to the total energy and J values, and not sensitive to the initial vibrational quantum number of the reagents.

However, as we have seen, the less-direct group of trajectories is sensitive to the initial O_2 vibrational excitation in several different temperature ranges, while the more-direct group of trajectories, on both the DMBE IV PES and the MB PES, exhibits no significant enhancement of reactivity due to the initial vibrational excitation of the O_2 reagent compared to the effect of a simple temperature increase. The less-direct group seems to "remember" the initial vibrational excitation despite the fact that these trajectories are less-direct, and consequently, may be more affected by the relatively deep HO_2 potential energy well. For the less-direct group of trajectories, Figures 3 and 4 indicate that the addition of energy in the form of temperature changes causes the rate coefficients to decrease. This behavior is typical of addition−elimination reactions in which the addition of energy decreases the probability of forming a reactive complex.[159] Increasing the initial O_2 vibrational excitation (i.e. increasing the reagent vibrational energy) also increases the rate coefficient. Consequently, there is a modest overall vibrational enhancement of reaction 1.

In Figure 5, the rate coefficients for the more-direct group of trajectories calculated on the MB PES are plotted at a function of E_{tot}. Comparing the rate coefficients from the less-direct group of trajectories with these data indicates that increasing either the initial O_2 vibrational excitation or temperature cause much larger effects in more-direct group of trajectories. This behavior is consistent with a chemically activated process in which the probability of overcoming the reaction endoergicity is directly related to the available energy.[159] With more energy available, there is a greater number of collisions that lead to products. The case of $T = 1000$ K is particularly noteworthy. Increasing the temperature from 1000 K causes a very large increase in the rate coefficient, substantially greater than that caused by initial O_2 vibrational excitation. For $T = 2000$ K and greater, the effect on the rate coefficient of increasing temperature is roughly comparable to the effect of initial O_2 vibrational excitation. It is important to understand more clearly why the effect of increasing temperature is so dramatic below $T = 2000$ K.

In an attempt to understand the distinction in the dynamical behavior of the two groupings of trajectories on each PES, the data in Table 5 provide some insight. At $T = 1000$ K and $v = 6$ on the MB PES, 70% of the more-direct but only 51% of the less-direct reactive trajectories formed O + OH products with less than ZPE in the OH diatom. On the DMBE IV PES, the corresponding numbers are 76% and 48%. The data from the table also show a general trend on both PESs that the numbers of more-direct and less-direct reactive trajectories forming O + OH products with less than ZPE in the OH bond decrease as both temperature and initial O_2 vibrational quantum number increase. However, with only six exceptions on the MB PES (and none on the DMBE IV PES), the percent of more-direct reactive trajectories failing to produce OH with at least ZPE is always greater than that of the less-direct reactive trajectories.

These observations suggest that the intramolecular transfer of vibrational energy between the initially excited O_2 bond and the newly formed OH bond is inefficient on the time scale of the more-direct reactive trajectories. This inefficiency offers a possible explanation for the previous observation that the more-direct reactive trajectories are not sensitive to the initial vibrational excitation of the O_2 reagent, whereas the less-direct reactive trajectories seem to "remember" the initial O_2 vibrational excitation. Teitelbaum et al.[12] also note the inefficient energy transfer in reactions involving the O_2 diatom. Lemon and Hase,[160] pointing to the work of Davis and Gray,[161] suggest that the presence of quasiperiodic and "vague tori" trajectories in the HO_2* (the rovibrationally excited complex) phase space could create a bottleneck to intramolecular vibrational energy transfer between the O_2 coordinate and the OH coordinate. However, the conclusions of Dobbyn et al.[124,125,127] noted earlier contradict this interpretation. Consequently, the question of vibrational intramolecular energy transfer requires further study.

The possible inefficiency of intramolecular energy transfer on the time scale of the more-direct group of trajectories also offers a possible explanation for the observation that, especially at low temperatures, the over-all rate coefficient for reaction 1 is determined primarily by the less-direct group of trajectories (see Figures 6 and 7). It appears that the more-direct trajectories do not efficiently transfer energy from the O_2 coordinate to the OH coordinate, and hence, do not contribute to the over-all reaction rate. However, on the MB PES at $T = 4000$ K (Figure 8) and for higher O_2 vibrational excitation ($v = 9$ and 10), it appears that the apparent transfer inefficiency is outweighed by the availability of sufficient energy. To the extent that the less-direct group of trajectories may be more greatly affected by the relatively deep HO_2 potential energy well, Figures 6 and 7 indicate that this potential energy well may play a significant role in determining the rate of reaction 1, particularly at low temperatures. As the temperature and quantum number increase, this role diminishes and the total rate coefficient is determined more importantly by the more-direct trajectories. On the DMBE IV PES, the question is not so simply determined, as Figure 9 indicates. In this case, even at high temperatures and high levels of O_2 vibrational excitation, the more-direct and less-direct groups of trajectories contribute nearly equally to the total rate of reaction 1. At the very least we must conclude that, at least qualitatively, the deep potential energy well must play a different role on the two PESs.

There are two distinct possibilities. On one hand, the behavior observed here may be a reflection of a physically real limitation of transferring energy to the forming OH bond from a highly excited diatom whose component atoms are significantly more massive than the H-atom. As a result, on the time scale of the more-direct reactive trajectories, energy transfer is inefficient. On the other hand, the observed behavior raises a concern about

the effectiveness of both the MB PES model and the DMBE IV PES model to represent the microscopic dynamics involving highly excited O_2 molecules. As noted by Kendrick and Pack,[115] the MB PES possesses several deficiencies: a barrier in the entrance channel along the MEP; an incorrect well-depth for the HO_2 radical; a cusp instead of a smooth saddle for the exchange of the H-atom between the two O-atoms in HO_2; and the O + OH valley is an extrapolation not based on ab initio calculations. While the DMBE IV PES is considered to be the "...most accurate potential energy surface to date for the present purposes",[12] it too suffers from some limitations as Yang and Klippenstein[117] have noted. A thorough understanding of the coupling between the O_2 and the OH bonds is crucial to the development of models that accurately reflect the physical behavior of a reacting system. Further, as noted above, Sultanov and Balakrishnan[138] reported that the rate coefficients computed with the Harding, Troe, and Ushakov PES are approximately 50% larger than those computed on the DMBE IV PES.

V. Summary

This study has examined the effect of reagent vibrational excitation on the rate of reaction 1. Quasiclassical trajectories using the VENUS96 computer code have been computed on the MB PES (as contained in the POTLIB 2001 PES library) and the DMBE IV PES for the $H + O_2 \Leftrightarrow OH + O$ reaction with the nonrotating ($J = 0$) O_2 reagent vibrationally excited to levels $v = 6, 7, 8, 9, 10$. The calculations were completed at four different temperatures: 1000, 2000, 3000, and 4000 K. The vibrational energy levels were selected by using a semiclassical EBK quantization procedure while the relative translational energy was sampled from a Boltzmann distribution. The less-direct group of trajectories is sensitive to the initial O_2 vibrational excitation in several different temperature ranges. The more-direct group of trajectories does not exhibit this behavior. While the rate coefficient for the formation of the OH + O products is seen to increase monotonically with quantum number and nearly monotonically with temperature, the less-direct and more-direct groups of trajectories differ in their contribution to the total rate coefficient for reaction 1. In particular, at $T = 4000$ K, the two PESs used in this work differ dramatically in the roles of the less-direct and more-direct trajectories. Both of these observations may be understood in terms of an inefficient intramolecular energy transfer between the vibrationally excited O_2 bond and the forming OH bond.

The research reported here represents an initial attempt to elucidate the effects of reagent vibrational energy on the rate of reaction 1 for high levels of vibrational excitation. The use of the two well-known PESs, the MB PES and the DMBE IV, provides the opportunity for a direct comparison of the effects of the O_2 vibrational excitation. It is critical that the investigation of the effects of reagent vibrational excitation in reaction 1 be further studied on newly developed PESs for this reaction. Further, an examination of the case of the rotating O_2 diatom ($J > 0$) is in order. A detailed analysis of the microscopic dynamics of the reactants in the HO_2 potential energy well will also be necessary to delineate the efficiency of intramolecular vibrational energy transfer. Understanding this efficiency is critical to developing a more complete picture of the sensitivity of less-direct trajectories to the initial vibrational excitation of the O_2 reagent and the differing contributions of the less-direct and more-direct trajectories to the total rate coefficient of reaction 1. Finally, a careful analysis of this intramolecular vibrational energy transfer process is essential to the development of highly accurate PES models of reaction 1.

Last, this study has compared only two PESs, a comparison greatly facilitated by the POTLIB 2001 PES Library. The library reduced the effort to utilize two PESs in a single study. Under the best of circumstances, future additions to the POTLIB 2001 PES Library should encourage additional comparative studies among multiple PESs.

Acknowledgment. R.J.D. wishes to acknowledge very helpful comments and insights from Dr. Albert F. Wagner of Argonne National Laboratory. Additionally, R.J.D. thanks Dr. Wagner for research support through DOE Contract 2F-01802, which has made continued work to extend the POTLIB 2001 Library possible. Finally, R.J.D. acknowledges the donors of the Petroleum Research Fund, administered by the American Chemical Society, for partial support of this research and the Chemistry Department of IPFW for providing a portion of the computational resources used to complete this work.

References and Notes

(1) Hou, H.; Huang, Y.; Gulding, J.; Rettner, C. T.; Auerbach, D. J.; Wodtke, A. M. *Science* **1999**, *284*, 1647.
(2) Levine, R. D.; Manz, J. *J. Chem. Phys.* **1975**, *63*, 4280 and references therein.
(3) Ben-Shaul, A.; Levine, R. D.; Bernstein, R. B. *J. Chem. Phys.* **1974**, *61*, 4937.
(4) Procaccia, I.; Levine, R. D. *J. Chem. Phys.* **1975**, *63*, 4261.
(5) Pollak, E.; Levine, R. D. *Chem. Phys. Lett.* **1976**, *39*, 199.
(6) Levine, R. D.; Bernstein, R. B.; Kahana, P.; Procaccia, I.; Upchurch, E. T. *J. Chem. Phys.* **1976**, *64*, 796.
(7) Kaplan, H.; Levine, R. D.; Manz, J. *Chem. Phys.* **1976**, *12*, 447.
(8) Oref, I.; Tardy, D. C. *Chem. Rev.* **1990**, *90*, 1407.
(9) Weston R. E.; Flynn, G. W. *Annu. Rev. Phys. Chem.* **1992**, *43*, 559.
(10) Mullin A. S.; Schatz, G. C., Eds. *Highly Excited Molecules*: *Relaxation, Reaction and Structure*; American Chemical Society: Washington, DC, 1997.
(11) Barker, J. R.; Yoder, L. M.; King, K. D. *J. Phys. Chem. A* **2001**, *105*, 796.
(12) Teitelbaum, H.; Caridade, P. J. S. B.; Varandas, A. J. C. *J. Chem. Phys.* **2004**, *120*, 10483.
(13) Crim, F. F. *J. Phys. Chem.* **1996**, *100*, 12725.
(14) Frost, R. J.; Smith, I. W. M. *Chem. Phys.* **1987**, *117*, 389.
(15) Miller, J. A. *J. Chem. Phys.* **1986**, *84*, 6170.
(16) Varandas, A. J. C. *J. Phys. Chem. A* **2004**, *108*, 758.
(17) Varandas, A. J. C. *J. Chem. Phys.* **1993**, *99*, 1076.
(18) Dieke, G. H.; Crosswhite, H. M. *J. Quant. Spectrosc. Radiat. Transfer* **1962**, *2*, 97.
(19) Foner, S. N.; Hudson, R. L. *J. Chem. Phys*. **1962**, *36*, 2681.
(20) Milligan, D. E.; Jacox, M. E. *J. Chem. Phys*. **1963**, *38*, 2627.
(21) Getzinger, R. W.; Blair, L. S. *Combust. Flame* **1969**, *13*, 271.
(22) Krupenie, P. H. *J. Phys. Chem. Ref. Data* **1972**, *1*, 423.
(23) Friswell, N. S.; Sutton, M. M. *Chem. Phys. Lett*. **1972**, *15*, 108.
(24) Jacox, M. E.; Milligan, D. E. *J. Mol. Spectrosc*. **1972**, *42*, 495.
(25) Paukert, T. E.; Johnston, H. S. *J. Chem. Phys*. **1972**, *56*, 2824.
(26) Kurylo, M. J. *J. Phys. Chem*. **1972**, *76*, 3518.
(27) Ahumada, J. J.; Michael, J. V.; Osborne, D. T. *J. Chem. Phys*. **1972**, *57*, 3736.
(28) Smith, D. W.; Andrews, L. *J. Chem. Phys*. **1974**, *60*, 81.
(29) Wong, W.; D. D. Davis, D. D. *Int. J. Chem. Kinet*. **1974**, *6*, 401.
(30) Beers, Y.; Howard, C. J. *J. Chem. Phys*. **1976**, *64*, 1541.
(31) Slack, M. W. *Combust. Flame* **1977**, *28*, 241.
(32) Johns, J. W. C.; McKellar, A. R. W.; Riggin, M. J. *J. Chem. Phys*. **1978**, *68*, 3957.
(33) Barnes, C. E.; Brown, J. M.; Carrington, A.; Pinkstone, J.; Sears, T. J.; Thistlewaite, P. J. *J. Mol. Spectrosc*. **1978**, *72*, 86.
(34) Deleted in proof.
(35) Coxon, J. A.; Sastry, K. L. V. N.; Austin, J. A.; Levy, D. H. *Can. J. Phys*. **1979**, *57*, 619.
(36) Coxon, J. A. *Can. J. Phys*. **1980**, *58*, 933.
(37) Howard, C. J. *J. Am. Chem. Soc*. **1980**, *102*, 6937.
(38) Nagai, K.; Endo, Y.; Hirota, E. *J. Mol. Spectrosc*. **1981**, *89*, 520.
(39) Charo, A.; De Lucia, F. C. *J. Mol. Spectrosc*. **1982,** *94*, 426.
(40) Yamada, C.; Endo, Y.; Hirota, E. *J. Chem. Phys*. **1983**, *78*, 4379.
(41) Holstein, K. J.; Fink, E. H.; Wildt, J.; Winter, R.; Zabel, F. *J. Phys. Chem*. **1983**, *87*, 3943.
(42) Lubic, K. G.; Amano, T.; Uehara, H.; Kawaguchi, K.; Hirota, E. *J. Chem. Phys*, **1984**, *81*, 4826.

(43) Uehara, H.; Kawaguchi, K.; Hirota, E. *J. Chem. Phys*. **1985**, *83*, 5479.
(44) Troe, J. *J. Phys. Chem*. **1986**, *90*, 3485.
(45) Jacox, M. E. *J. Phys. Chem. Ref. Data* **1988**, *17*, 269.
(46) Christensen, H.; Sehested, K. *J. Phys. Chem*. **1988**, *92*, 3007.
(47) Schwab, J. J.; Brune, W. H.; Anderson, J. G. *J. Phys. Chem*. **1989**, *93*, 1030.
(48) Nelson, D. D.; Zahniser, M. S. *J. Mol. Spectrosc*. **1991**, *150*, 527.
(49) Adhikari N.; Hamilton, I. *J. Phys. Chem*. **1991**, *95*, 6470.
(50) Jacobs, A.; Volpp, H.-R.; Wolfrum, J. *Chem. Phys. Lett*. **1991**, *177*, 200.
(51) Burkholder, J. B.; Hammer, P. D.; Howard, C. J.; Towle, J. P.; Brown, J. M. *J. Mol. Spectrosc*. **1992**, *151*, 493.
(52) Kessler, K.; Kleinermanns, K. J. *J. Chem. Phys*. **1992**, *97*, 374.
(53) Seeger, S.; Sick, V.; Volpp, H.-R.; Wolfrum, J. *Isr. J. Chem*. **1994**, *34*, 5.
(54) Sawyer, D. T. *J. Phys. Chem*. **1989**, *93*, 7977.
(55) Fisher, E. R.; Armentrout, P. B. *J. Phys. Chem*. **1990**, *94*, 4396.
(56) Holmes, J. L.; Lossing, F. P.; Mayer, P. M. *J. Am. Chem. Soc*. **1991**, *113*, 9723.
(57) Schott, G. L. *Combust. Flame* **1973**, *21*, 357.
(58) Frank, P.; Just, Th. *Ber. Bunsen-Ges. Phys. Chem*. **1985**, *89*, 181.
(59) Cobos, C. J.; Hippler, H.; Troe, J. *J. Phys. Chem*. **1985**, *89*, 342.
(60) Hsu, K.-J.; Durant, J. L.; Kaufman, F. *J. Phys. Chem*. **1987**, *91*, 1895.
(61) Fuji, N.; Shin, K. S. *Chem. Phys. Lett*. **1988**, *151*, 461.
(62) Pirraglia, A. N.; Michael, J. V.; Sutherland, J. W.; Klemm, R. B. *J. Phys. Chem*. **1989**, *93*, 282.
(63) Hsu, K.-J.; Anderson, S. M.; Durant, J. L.; Kaufman, F. *J. Phys. Chem*. **1989**, *93*, 1018.
(64) Masten, D. A.; Hanson, R. K.; Bowman, C. T. *J. Phys. Chem*. **1990**, *94*, 7119.
(65) Yuan, T.; Wang, C.; Yu, C.-L.; Frenklach, M.; Rabinowitz, M. J. *J. Phys. Chem*. **1991**, *95*, 1258.
(66) Rubahn, H.-G.; van der Zande, W. J.; Zhang, R.; Bronikowski, M. J.; Zare, R. N. *Chem. Phys. Lett*. **1991**, *186*, 154.
(67) Shin, K. S.; Michael, J. V. *J. Chem. Phys*. **1991**, *95*, 262.
(68) Du, H.; Hessler, J. P. *J. Chem. Phys*. **1992**, *96*, 1077.
(69) Hughes, K. J.; Lightfoot, P. D.; Pilling, M. J. *Chem. Phys. Lett*. **1992**, *191*, 581.
(70) Carleton, K. L.; Kessler, W. J.; Martinelli, W. J. *J. Phys. Chem*. **1993**, *97*, 6412.
(71) Yu, C.-L.; Frenklach, M.; Masten, D. A.; Hanson, R. K.; Bowman, C. T. *J. Phys. Chem*. **1994**, *98*, 4770.
(72) Baulch, D. L.; Cox, R. A.; Cutzen, P. J.; Hampson, R. F., Jr.; Kerr, J. A.; Troe, J.; Watson, R. T. J. *Phys. Chem. Ref. Data* **1982**, *11*, 327.
(73) Cohen, N.; Westberg, K. R. *Chemical Kinetic Data Sheets for High-Temperature Chemical Reactions*; Aerospace Report No. ATR-82(7888)-3; Aerospace Corporation: El Segundo, CA, 1982.
(74) Cohen, N.; Westberg, K. R. *J. Phys. Chem. Ref. Data* **1983**, *12*, 531.
(75) Melius, C. F.; Blint, R. L. *Chem. Phys. Lett*. **1979**, *64*, 183.
(76) Komornicki, A.; Jaffe, R. L. *J. Chem. Phys*. **1979**, *71*, 2150.
(77) Walch, S. P.; Rohlfing, C. M.; Melius, C. F.; Bauschlicher, C. W. *J. Chem. Phys*. **1988**, *88*, 6273.
(78) Walch, S. P.; Rohlfing, C. M. *J. Chem. Phys*. **1989**, *91*, 2373.
(79) Walch, S. P.; Duchovic, R. J. *J. Chem. Phys.* **1991**, *94*, 7068.
(80) Bauschlicher, C. W.; Langhoff, S. R. *J. Chem. Phys.* **198**9, *90*, 3230.
(81) Francisco, J. S.; Zhao, Y. *Mol. Phys*. **1991**, *72*, 1207.
(82) Pastrana, M. R.; Quintales, L. A. M.; Brandao, J.; Varandas, A. J. C. *J. Phys. Chem.* **1990**, *94*, 8073.
(83) Sicilia, E.; Russo, N. *Mol. Phys*. **1992**, *76*, 1025.
(84) Bunker, P. R.; Hamilton, I. P.; Jensen, P. *J. Mol. Spectrosc*. **1992**, *155*, 44.
(85) Bauschlicher, C. W.; Partridge, H. *Chem. Phys. Lett*. **1993**, *208*, 241.
(86) Dobbs, K. D.; Dixon, D. A. *J. Phys. Chem*. **1994**, *98*, 4498.
(87) Lauderdale, W. J.; Cheng, V. G.; Wierschke, S. G. *J. Phys. Chem.* **1994**, *98*, 4502.
(88) Gauss, A., Jr. *J. Chem. Phys*. **1978**, *68*, 1689.
(89) Blint, R. L. *J. Chem. Phys*. **1980**, *73*, 764.
(90) Miller, J. A. J. *Chem. Phys.* **1981**, *74*, 5120.
(91) Miller, J. A. *J. Chem. Phys*. **1981**, *75*, 5349.
(92) Bottomley, M.; Bradley, J. N.; Gilbert, J. R. *Int. J. Chem. Kinet*. **1981**, *13*, 957.
(93) Miller, J. A.; Brown, N. J. *J. Phys. Chem*. **1982**, *86*, 772.
(94) Rai, S. N.; Truhlar, D. G. *J. Chem. Phys*. **1983**, *79*, 6046.
(95) Kleinermanns, K.; Schinke, R. *J. Chem. Phys*. **1984**, *80*, 1440.
(96) Lemon, W. J.; Hase, W. L. *J. Phys. Chem*. **1987**, *91*, 1595.
(97) Ju, G.; Feng, D.; Cai, Z.; Dong, C. *Theor. Chim. Acta* **1988**, *74*, 403.
(98) Davidsson, J.; Nyman, G. *Chem. Phys.***1988**, *125*, 171.
(99) Quintales, L. A. M.; Varandas, A. J. C.; Alvarino, J. M. *J. Phys. Chem*. **1988**, *92*, 4552.
(100) Varandas, A. J. C.; Brandao, J.; Quintales, L. A. M. *J. Phys. Chem*. **1988**, *92*, 3732.
(101) Cobos, C. J. *Chem. Phys. Lett*. **1988**, *152*, 371.
(102) Markovic, N.; Nyman, G.; Nordholm, S. *Chem. Phys. Lett*. **1989**, *159*, 435.
(103) Schneider, F.; Zuelicke, L.; Chapuisat, X. *Mol. Phys*. **1990**, *71*, 17.
(104) Davidsson, J.; Nyman, G. *J. Chem. Phys*. **1990**, *92*, 2407.
(105) Nyman, G.; Davidsson, J. *J. Chem. Phys*. **1990**, *92*, 2415.
(106) Varandas, A. J. C.; Brandao, J.; Pastrana, M. R. *J. Chem. Phys*. **1992**, *96*, 5137.
(107) Zuhrt, C.; Zuelcke, L.; Chapuisat, X. *Chem. Phys*. **1992**, *166*, 1.
(108) Klimo, V.; Bittererova, M.; Biskupic, S.; Urban, J.; Nicov, M. *Collect. Czech. Chem. Commun*. **1993**, *58*, 234.
(109) Klimo, V.; Bittererova, M.; Biskupic, S.; Urban, J. *Chem. Phys*. **1993**, *173*, 367.
(110) Nyman, G. *Chem. Phys*. **1993**, *173*, 159.
(111) Pack, R. T.; Butcher, E. A.; Parker, G. A. *J. Chem. Phys*. **1993**, *99*, 9310.
(112) Duchovic, R. J.; Pettigrew, J. D. *J. Phys. Chem*. **1994**, *98*, 10794.
(113) Lauderdale, W. J.; Cheng, V. G.; Wierschke, S. G. *J. Phys. Chem*. **1994**, *98*, 4502.
(114) Zhang, D. H.; Zhang, J. Z. H. *J. Chem. Phys*. **1994**, *101*, 3671.
(115) Kendrick, B.; Pack, R. T *J. Chem. Phys*. **1995**, *102*, 1994.
(116) Pack, R. T.; Butcher, E. A.; Parker, G. A. *J. Chem. Phys*. **1995**, *102*, 5998.
(117) Yang, C.-Y.; Klippenstein, S. J. *J. Chem. Phys*. **1995**, *103*, 1.
(118) Dai, J.; Zhang, J. H. Z. *J. Chem. Phys*. **1996**, *104*, 3664.
(119) Kendrick, B.; Pack, R. T *J. Chem. Phys*. **1996**, *104*, 7502.
(120) Leforestier, C.; Miller, W. H. *J. Chem. Phys*. **1994**, *100*, 733.
(121) Viel, A.; Leforestier, C.; Miller, W. H. *J. Chem. Phys*. **1998**, *108*, 3489.
(122) Germann, T. C.; Miller, W. H. *J. Phys. Chem. A* **1997**, *101*, 6358.
(123) Skinner, D. E.; Germann, T. C.; Miller, W. H. *J. Phys. Chem A* **1998**, *102*, 3828.
(124) Dobbyn, A. J.; Stumpf, M.; Keller, H.-M.; Hase, W. L.; Schinke, R. *J. Chem. Phys*. **1995**, *102*, 5867.
(125) Dobbyn, A. J.; Stumpf, M.; Keller, H.-M.; Schinke, R. *J. Chem. Phys*. **1995**, *103*, 9947.
(126) Song, K.; Peslherbe, G. H.; Hase, W. L.; Dobbyn, A. J.; Stumpf, M.; Schinke, R. *J. Chem. Phys*. **1995**, *103*, 8891.
(127) Dobbyn, A. J.; Stumpf, M.; Keller, H.-M.; Schinke, R. *J. Chem. Phys*. **1996**, *104*, 8357.
(128) Meijer, A. J. H. M.; Goldfield, E. M. *J. Chem. Phys.* **1998**, *108*, 5404.
(129) Meijer, A. J. H. M.; Goldfield, E. M. *J. Chem. Phys.* **1999**, *110*, 870.
(130) Goldfield, E. M.; Meijer, A. J. H. M. *J. Chem. Phys.* **2000**, *113*, 11055.
(131) Bajeh, M. A.; Goldfield, E. M.; Hanf, A.; Kappel, C.; Meijer, A. J. H. M.; Volp, H.-R.; Wolfrum, J. *J. Phys. Chem. A* **2001**, *105*, 3359.
(132) Deleted in proof.
(133) Meijer, A. J. H. M.; Goldfield, E. M. *Phys. Chem. Chem. Phys*. **2001**, *3*, 2811.
(134) Harding, L. B.; Troe, J.; Ushakov, V. G. *Phys. Chem. Chem. Phys.* **2000**, *2*, 631.
(135) Harding, L. B.; Maergoiz, A. I.; Troe, J.; Ushakov, V. G. *J. Chem. Phys.* **2001**, *113*, 11019.
(136) Troe, J.; Ushakov, V. G. *J. Chem. Phys.* **2001**, *115*, 3621.
(137) Rusic, B.; Feller, D.; Dixon, D. A.; Peterson, K. A.; Harding, L. B.; Asher, R. L.; Wagner, A. F. *J. Chem. Phys.* **2001**, *105*, 1.
(138) Sultanov, R. A.; Balakrishnan, N. *J. Phys. Chem. A* **2004**, *108*, 8759.
(139) Troe, J. *Z. Phys. Chem.* **2003**, *217*, 1303.
(140) Duchovic, R. J.; Volobuev, Y. L.; Lynch, G. C.; Truhlar, D. G.; Allison, T. C.; Wagner, A. F.; Garrett, B. C.; Corchado, J. *Comput. Phys. Commun*. **2002**, *144***,** 169.
(141) Hase, W. L.; Duchovic, R. J.; Hu, X.; Komornicki, A.; Lim, K. F.; Lu, D.-h.; Peslherbe, G. H.; Swamy, K. N.; Vande Linde, S. R.; Varandas, A. J. C.; Wang, H.; Wolf, R. J. VENUS96: A General Chemical Dynamics Computer Program *QCPE Bull*. **1996**, *16*, 43.
(142) Bowman, J. M.; Gazdy, B.; Sun, Q. *J. Chem. Phys.* **1989**, *91*, 2859.
(143) Miller, W. H.; Hase, W. L.; Darling, C. L. *J. Chem. Phys.* **1989**, *91*, 2863.
(144) Alimi, R.; Garcia-Vela, A.; Gerber, R. B. *J. Chem. Phys.* **1992**, *96*, 2034.
(145) Varandas, A. J. C.; Marques, J. M. C. *J. Chem. Phys.* **1994**, *100*, 1908.
(146) Varandas, A. J. C. *Chem. Phys. Lett.* **1994**, *225*, 18.
(147) Peslherbe, G. H.; Hase, W. L. *J. Chem. Phys.* **1994**, *100*, 1179.

(148) Ben-Nun, M.; Levine, R. D. *J. Chem. Phys.* **1994**, *101*, 8768.
(149) Kumar, S.; Sathyamurty, N.; Ramaswamy, *J. Chem. Phys.* **1995**, *103*, 6021.
(150) Lim, K. F.; McCormack, D. A. *J. Chem. Phys.* **1995**, *102***,** 1705.
(151) McCormack, D. A.; Lim, K. F. *J. Chem. Phys.* **1995**, *103*, 1991.
(152) Guo, Y.; Thompson, D. L.; Sewell, T. D. *J. Chem. Phys.* **1996**, *104*, 576.
(153) Peslherbe, G. H.; Hase, W. L. *J. Chem. Phys.* **1996**, *104*, 9445.
(154) Shen, D. L.; Pritchard, H. O. *J. Chem. Soc., Faraday Trans.* **1996**, *92*, 1297.
(155) Shen, D. L.; Pritchard, H. O. *J. Chem. Soc., Faraday Trans.* **1996**, *92*, 4357.
(156) Lim, K. F. *J. Chem. Soc., Faraday Trans.* **1997**, *93*, 669.
(157) McCormack, D. A.; Lim, K. F. *Phys. Chem. Chem. Phys.* **1999**, *1*, 1.
(158) Teitelbaum, H.; Lifshitz, A. *Phys. Chem. Chem. Phys.* **2000**, *2*, 687.
(159) Wagner, A. F. Private communication.
(160) Lemon, W. J.; Hase, W. L. *J. Phys. Chem.* **1987**, *91*, 1596.
(161) Davis, M. J.; Gray, S. K. *J. Chem. Phys.* **1986**, *84*, 5389.